

Superluminous supernova search with PineForest

T. Majumder^a, M. V. Pruzhinskaya^b, E. E. O. Ishida^b, K. L. Malanchev^c, T. A. Semenikhin^{d,e}

^a*University of Lethbridge, 4401 University Dr W, Lethbridge, AB T1K 3M4, Alberta, Canada*

^b*Université Clermont Auvergne, CNRS/IN2P3, LPCA, Clermont-Ferrand, F-63000, France*

^c*McWilliams Center for Cosmology and Astrophysics, Carnegie Mellon University, 5000 Forbes Avenue, Pittsburgh, PA 15213, Pennsylvania, USA*

^d*Lomonosov Moscow State University, Sternberg astronomical institute, Universitetsky pr. 13, Moscow, 119234, Russia*

^e*Lomonosov Moscow State University, Faculty of Physics, Leninskie Gory, 1-2, Moscow, 119991, Russia*

Abstract

The advent of large astronomical surveys has made available large and complex data sets. However, the process of discovery and interpretation of each potentially new astronomical source is, many times, still handcrafted. In this context, machine learning algorithms have emerged as a powerful tool to mine large data sets and lower the burden on the domain expert. Active learning strategies are specially good in this task. In this report, we used the PineForest algorithm to search for superluminous supernova (SLSN) candidates in the Zwicky Transient Facility. We showcase how the use of previously confirmed sources can provide important information to boost the convergence of the active learning algorithm. Starting from a data set of \sim 14 million objects, and using 8 previously confirmed SLSN light curves as priors, we scrutinized 120 candidates and found 8 SLSN candidates, 2 of which have not been reported before (AT 2018moa and AT 2018mob). These results demonstrate how existing spectroscopic samples can be used to improve the efficiency of active learning strategies in searching for rare astronomical sources.

Keywords: Supernovae, Methods, Statistical, Machine Learning, Anomaly Detection

1. Introduction

Large scale sky surveys, of which one of the most prolific examples is the Zwicky Transient Facility (ZTF, Bellm et al., 2018), have revolutionized the way astronomers interact with the data. Given that each data release (DR) contains a few billion light curves (Malanchev et al., 2023), visually screening the entire data set is not feasible. In this context, automatic machine learning algorithms offer the possibility to quickly classify large data sets (Baron, 2019). However, such algorithms traditionally require a large number of previously labeled examples for training. This might not be a problem if the target of classification is a well established, and deeply scrutinized, class of astronomical objects. On the other hand, if the goal is to find rare or not well known objects, for which only a small spectroscopically confirmed sample is available, the task becomes much more difficult.

Anomaly detection (AD) algorithms are designed to automatically identify samples which deviate from the bulk of the data or those unlikely to be generated by the same underlying statistical distribution used to describe the overall behavior of a large data set (Xiong et al., 2010). Such strategies have been extensively exploited in recent literature, and have proven to be successful when applied to a wide range of wavelengths and data formats in astronomy (see e.g., Forestano et al., 2023; Mesaricik et al., 2023; Parmiggiani et al., 2023; Perez-Carrasco et al., 2023; Aleo et al., 2024; Horton et al., 2024). However, given the peculiarities of astronomical data, such examples will frequently correspond to non-physical artifacts (noise, instrument failures, spurious detections due to weather conditions, among

others). Despite its clear success, AD applied to astronomical data is known to generate a significant fraction of non-physical outliers (Sánchez-Sáez et al., 2021; Malanchev et al., 2021).

In order to identify scientifically interesting anomalies, feedback from the domain expert is paramount. This is where active learning (AL, Settles, 2012) strategies play an important role. AL is a class of machine learning algorithms where expert feedback is used on-the-fly to impose modifications in the training sample, or in the hyperparameters of a particular machine learning model, thus allowing for incremental increase in performance. When used in the context of AD, these learning strategies allow the construction of personalized models, targeting the specific anomalies which satisfy the user's definition. Active AD algorithms like, Active Anomaly Discovery (AAD, Das et al., 2017; Ishida et al., 2021) and Astronomaly (Lochner and Bassett, 2021), have been applied to different astronomical data sets (see e.g., Pruzhinskaya et al., 2023; Andersson et al., 2024; Semenikhin et al., 2024; Voloshina et al., 2024) showcasing their potential in helping select scientifically interesting objects which can posteriorly be scrutinized by the expert.

Despite their undeniable success, all active learning strategies when applied to a new data set require at least a few iterations during which the expert needs to go through some obviously non-interesting candidates. This *burn-in* period is necessary to start the fine tuning process of selecting candidates satisfying the user's requirements. Although this stage is unavoidable, it is possible to boost the convergence of the algorithm by providing examples of what the expert is searching for before the actual learning loop starts. In this work, we showcase one possible application of this strategy while searching

for superluminous supernova (SLSN) in the ZTF DR8.

Superluminous supernovae are transients brighter ($L_{\max} \gtrsim 10^{44}$ erg s $^{-1}$) than typical supernovae and show a wide range of photometric and spectroscopic properties (Gal-Yam, 2012, 2019). The first reports of their detection date from the turn of the century, however, they only became more frequent with the arrival of systematic sky surveys. Given their high luminosity, it is possible to detect them at relatively high redshifts, thus enabling their use in the study of star formation in the early Universe ($z \geq 2$), the interstellar medium or even in cosmological applications (Moriya et al., 2018).

Given that SLSNe are relatively rare and their consequent low incidence in ZTF DRs, they constitute a good science case to demonstrate how the use of already known examples can help boost results from active learning. We present results from applying the PineForest algorithm (Kornilov et al., 2024, Korolev et al., - in prep.) enhanced with previously labeled examples. The characteristics of the data set are described in Section 2 and our complete analysis pipeline is described in Section 3. We present our findings in Section 4 and conclusions in Section 5.

2. Data

The Zwicky Transient Facility (Bellm et al., 2018) constitutes a public, multi-band survey conducted in the $\{zg, zr, zi\}$ passbands, covering the entire northern sky within the wavelength range [4000 Å, 9000 Å]. It has a large instantaneous field of view CCD camera, which effectively leverages the entire focal plane (~ 47 deg 2) of the 48-inch Samuel Oschin Telescope at Palomar, resulting in a survey footprint which varies between 1000 and 2000 square degrees, depending on the season¹. ZTF conducts bi-monthly public data releases (DRs), providing high-quality and reliable data products to enable time-domain science. In this work, we analyzed private and public data from ZTF DR8, which spans from March 2018 to September 2021 ($58194 \leq \text{MJD} \leq 58972$).

As a starting point, we used the data curated by Voloshina et al. 2024. We examined only the clear ($\text{catflags} = 0$) zr -band light curves containing at least 300 detections in each light curve. Moreover, we considered only sources with galactic latitude $b \geq 30^\circ$. This criterion aims to exclude galactic plane, then prioritizing the extragalactic transients. In total, we analyzed 13761212 ZTF object identifiers (OIDs).

2.1. Confirmed superluminous supernova sample

Our initial SLSN sample was constructed using spectroscopically confirmed SLSN from Transient Name Server² (TNS), resulting in 50 ZTF light curves. However, only 8 light curves (corresponding to 6 individual SLSNe) fulfilled our selection cuts and were available in the data set curated by Voloshina et al. (2024). The surviving SLSNe are listed in Table 1. We used these as a positive class priors initially given to the PineForest algorithm to search for new SLSN candidates.

Table 1: The prior list comprises 8 confirmed superluminous supernova light curves (corresponding to 6 individual SLSNe). SN 2018don is classified as an SLSN-I, and we referenced the three different ZTF OIDs for SN 2018don from distinct ZTF Field IDs – 821, 791, and 792. We assembled all the ZTF OIDs in the prior list based on their availability in the ZTF DR8 feature file curated by Voloshina et al. (2024).

TNS Name	Type	ZTF OID(s)
SN 2018don	SLSN-I	821202400019642, 791213100013510, 792216100000865
SN 2018hxe	SLSN-II	822210300019023
SN 2018kyt	SLSN-I	790212100011207
SN 2018lng	SLSN-II	789212300014493
SN 2019aje	SLSN-II	756207300001552
SN 2019fdr	SLSN-II	634210400021472

3. Methodology

In this study, to identify new SLSN candidates, we started our investigation using the features from (Voloshina et al., 2024). Features from the spectroscopically confirmed SLSNe were presented to the PineForest algorithm as priors. Subsequently, we performed the traditional active learning loop using PineForest.

3.1. Feature set

We used pre-processed data with 53 extracted features from the ZTF DR8 (Voloshina et al., 2024). These features were computed using the light-curve³ package developed by Malanchev et al. (2021). The feature set encompasses both magnitude and flux properties, such as Amplitude, Kurtosis, and Standard Deviation. A complete list of the distribution of these features and the priors is illustrated in Figures B.4-B.8 in Appendix B. Subsequently, we conducted a comprehensive analysis of each light curve based on these features. This ensemble of features elucidates different aspects of the light curve shape, with the tails of feature distributions highlighting objects with less common light curve properties or potential outliers in our data set.

3.2. PineForest

We employed the PineForest algorithm, a component of the CONIFEREST⁴ package (Kornilov et al., 2024) in our SLSN search. PineForest is an adaptive learning mechanism that distinguishes itself from the traditional Isolation Forest (IF, Liu et al. 2008) by eliminating the less influential trees. At each iteration, the object with higher anomaly score is shown to the expert, who is asked to reply YES/NO. If the expert replies YES, the object with second highest anomaly score is shown. If the feedback is NO, the algorithm proceeds to eliminate trees which attributed a high anomaly score to that particular sample. A new set of trees are generated and the scores are recalculated. The procedure continues until the maximum budget

¹https://irsa.ipac.caltech.edu/data/ZTF/docs/releases/dr07/ztf_release_notes_dr07.pdf

²<https://www.wis-tns.org/>

³<https://github.com/light-curve/light-curve-python>

⁴<https://coniferest.snad.space/en/latest/>

stipulated by the user, with each iteration fine tuning the set of surviving trees which reflects the feedback from the expert. This approach results in a personalized model that is less likely to assign high anomaly scores to objects not of primary interest to the expert. A comprehensive description of the PineForest algorithm is available in (Kornilov et al., 2024, Korolev *et al.*, - in prep.).

The scoring mechanism of this algorithm is defined as,

$$y_j = \begin{cases} 1, & \text{if } x_i \text{ is normal,} \\ 0, & \text{if } x_i \text{ is unlabeled,} \\ -1, & \text{if } x_i \text{ is an anomaly} \end{cases} \quad (1)$$

$$\text{score}(T_i) = \sum_{j=1}^N y_j \cdot d(T_i(x_j)), \quad (2)$$

where T_i is the i^{th} tree in the forest, y_j is the label assigned to each sample x_j , and $d(T_i(\cdot))$ is the depth of the x_j sample in the tree.

In this work, we also use one additional feature from the CONIFEREST package: the possibility to give examples of the positive class to be used as priors, before the beginning of the iterative learning loop. In this option, the algorithm takes a list of examples (Table 1) which have already been scrutinized and classified. At first, it grows random decision trees, then uses the provided labels to filter out trees whose resulting anomaly score do not agree with the reported label. This procedure is repeated sequentially for all examples and only after this the iterative loop starts to pose questions to the expert. This procedure takes advantage of legacy data to pre-train the forest and thus lower the number of loops necessary to start showing interesting examples to the expert.

3.3. Visual inspection

At each iteration, the PineForest algorithm presents a candidate to the expert. In return, it expects a boolean answer regarding whether the ZTF OID is considered a scientifically interesting anomaly. The expert will then search for information to support their answer, which should be based on the light curve behavior and auxiliary data, such as literature reviews, community engagement, cross-matching with established databases and catalogs, and assessments against theoretical models.

To facilitate this human-in-the-loop feedback, we utilized the SNAD ZTF Viewer⁵ Malanchev et al. (2021), a web interface developed to support the domain expert analysis. Each OID in the Viewer is represented as multi-band light curves, providing access to individual exposure images and the Aladin Sky Atlas (Boch et al., 2014; Bonnarel, F. et al., 2000). Additionally, it provides cross-matching with various other catalogs and databases of stars and transients, including SIMBAD and VizieR databases (Wenger et al., 2000), AAVSO VSX (Watson et al., 2022), Pan-STARRS DR2 (Flewelling et al., 2020), Gaia DR3

(Gaia Collaboration et al., 2023), and ZTF alert brokers⁶⁷⁸.

4. Results

We run PineForest with a budget of 120 objects. During the human-in-the-loop analysis by the domain experts, we identified 10 OIDs, for which we responded YES in the PineForest interface, designating them as anomalous. Among these 10 candidates, we have identified 8 potential SLSNe. The remaining object, AT 2018lus (OID: 763203200003773), associated with a radio source NVSS J172435+452013, may represent a potential Active Galactic Nucleus (AGN). Additionally, we identified SN 2018dfa twice during our investigation, each associated with a different OID (794208200041246 and 794208200022136).

Among the 8 SLSNe candidates, only one (SN 2018fcg) is a known, spectroscopically confirmed, SLSN. Three objects have spectroscopic redshifts, while the remaining five only have photometric redshifts. The zr -band light curves of the candidates, after subtracting the host galaxy's contamination, are shown in Figures 1 and 2. We employed Gaussian Process (GP) regression to model each light curve, to estimate the peak apparent magnitude ($m_{r, \text{peak}}^{\text{GP}}$) and the time of maximum ($t_{0, \text{peak}}^{\text{GP}}$). To assess the classification as an SLSN, we calculated the absolute magnitude using the formula:

$$M_{r, \text{peak}} = m_{r, \text{peak}} - 5 \lg D + 5 - A_r, \quad (3)$$

where A_r is the Milky Way (MW) foreground extinction in the r -band ($A_r = 2.271 \times E(B-V)$, Schlafly and Finkbeiner, 2011) and D is the luminosity distance to the object in Mpc, assuming a flat Λ CDM cosmology ($H_0 = 70 \text{ km s}^{-1} \text{ Mpc}^{-1}$, $\Omega_m = 0.30$). We did not apply any K-correction because the spectroscopic redshifts are relatively low, and the photometric redshifts have large uncertainties. Our goal is to provide a rough estimate and compare the peak magnitude against the threshold commonly used to define SLSNe. Specifically, we consider SNe with reported peak magnitudes of $M < -21$ mag in any band as superluminous (Gal-Yam, 2012).

Formally, 5 out of the 8 SLSN candidates meet this criterion; however, it is important to emphasize the large uncertainties for transients with only photometric redshifts. According to this definition, SN 2018dfa qualifies as a superluminous SN, although it is spectroscopically classified as an SN IIP in TNS (Fremling et al., 2018).

The application of prior knowledge within the PineForest active learning framework has facilitated the identification of 2 new supernova candidates, designated as ZTF18aaqlkkf/AT 2018moa⁹ and AT 2018mob¹⁰ (see Fig-

⁶<https://alerce.science/>

⁷<https://antares.noirlab.edu/>

⁸<https://fink-portal.org/>

⁹<https://www.wis-tns.org/object/2018moa>

¹⁰<https://www.wis-tns.org/object/2018mob>

⁵<https://ztf.snad.space>

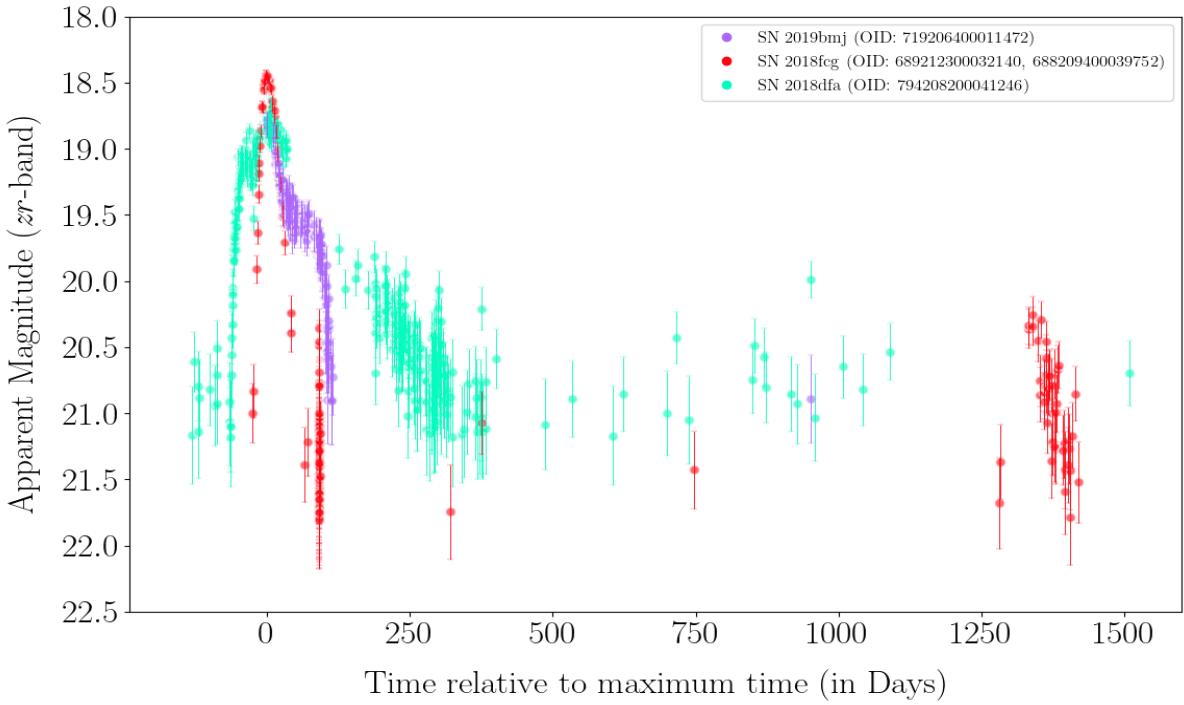


Figure 1: Superluminous supernova candidates with available spectroscopic redshift identified using the `PineForest` algorithm. Only the ZTF OIDs included in the `PineForest` outputs were used to construct the light curves, with the exception of SN 2018fgc, for which we used an additional OID: 688209400039752 to show the rise of the late bump in its second peak. The MW extinction is not taken into account.

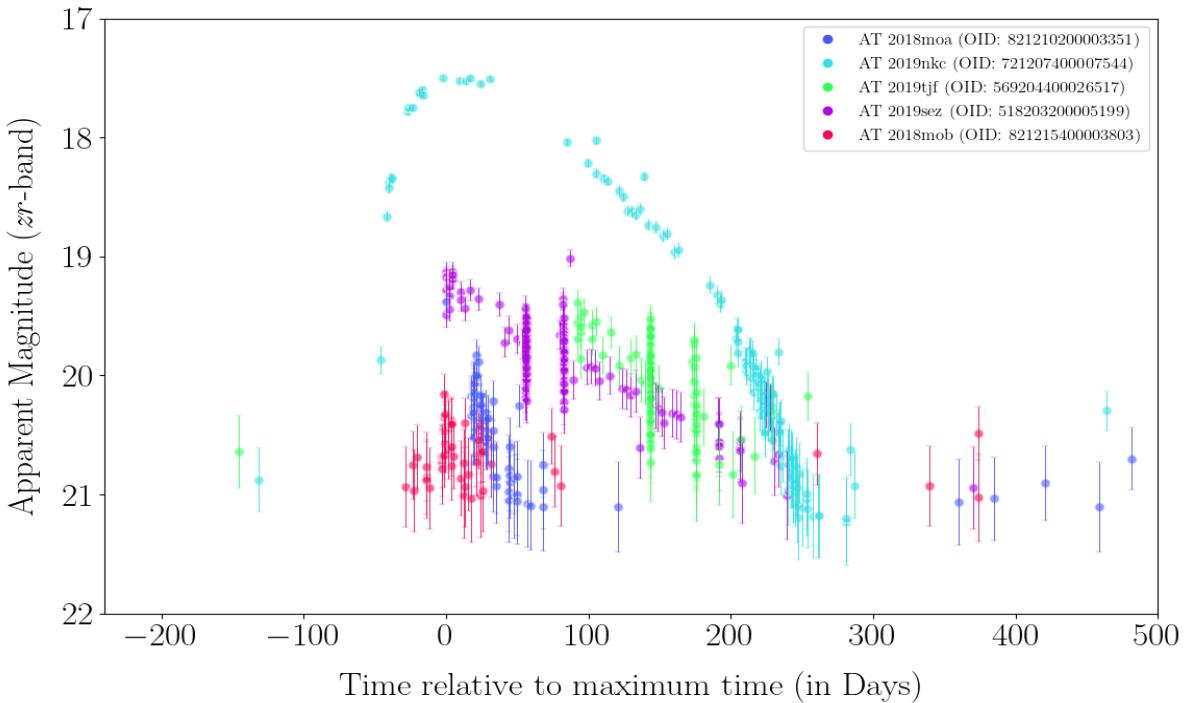


Figure 2: Superluminous supernova candidates with available photometric redshift identified using the `PineForest` algorithm. Only the ZTF OIDs included in the `PineForest` outputs were used to construct the light curves. The MW extinction is not taken into account.

ure 2), which have been formally reported to the TNS. AT 2018mob is missing in the official ZTF alert stream.

Table A.2 lists the summary of the 8 objects identified during our search. The first and second columns represent the TNS name and classification of each object. The third and fourth columns provides the equatorial coordinates, right ascension (RA) and declination (Dec), in degrees. The fifth column indicates the line-of-sight reddening within our galaxy, E(B-V) (Schlafly and Finkbeiner, 2011). The sixth column contains the spectroscopic or photometric redshifts of the objects. The seventh column presents the reference magnitude based on the Pan-STARRS DR2 (Flewelling et al., 2020) and ZTF reference magnitude used for correcting the host-galaxy contamination. The eight column represents the approximate absolute zr magnitude derived using Equation 3. The estimated GPs peak apparent magnitude ($m_{r,peak}^{GP}$) without MW extinction correction and the time of maximum in MJD ($t_{0,peak}^{GP}$) are listed in columns nine and ten. Column eleven lists all available ZTF OIDs for the zg , zr , and zi bands, with the highlighted OIDs corresponding to the PineForest outputs.

4.1. SN 2018fcg – ZTF18abmasep

Our investigation has led us to identify an additional anomalous multi-peaked light curve, SN 2018fcg, classified as a hydrogen-poor superluminous supernovae (SLSN-I), as reported at TNS (Fremling et al., 2018), which exhibits a peak magnitude of $M_{r,peak} = -21.62$ mag. This light curve is characterized by two peaks; the second peak is significantly dimmer than the first in the zr band and has not been announced before this study (see Figure 1). The prominent bumps observed in the late-time light curves could be due to the CSM interactions, as indicated by Smith et al. (2010). However, given such a long-lived light curve and the large gap between two peaks (> 1300 days), it is difficult to explain such behavior within the standard SLSN scenarios and this event can be something else (see also Pessi et al. 2024).

4.2. Other outliers

The majority of the PineForest run outputs were quasars (QSO) or QSO candidates, whose light curves can easily be mistaken for those of SLSNe. Additionally, the outliers included single stars, galaxies, artifacts, long-period variables, and known supernovae of classical types (Ia, II). Most of these objects exhibit broad light curves within the time range we examined. Figure 3 illustrates examples, including a known QSO and an AM Herculis-type variable.

5. Conclusions

This study introduces a novel approach to integrate prior knowledge as an additional information to aid convergence within an active learning pipeline, specifically designed to identify anomalous light curves. For the first time, the PineForest algorithm has been employed with priors to systematically search for potential superluminous supernova candidates within the Zwicky Transient Facility Data Release 8.

By considering merely 8 SLSNe light curves as priors, we identified 8 SLSNe candidates, including two new transients, AT 2018moa and AT 2018mob. Furthermore, we also discovered a re-brightening of SLSN-I, SN 2018fcg, which origin will be interesting to investigate in the future.

This strategy has the potential to yield further compelling discoveries regarding SLSNe once we use the entire prior catalog comprising 50 unique ZTF light curves for confirmed SLSN in the new data set curated for this research. Furthermore, this study can be extended beyond the identification of SLSNe. The methodology developed herein can be adapted to address various scientific problems across various domains, demonstrating the versatility and potential impact of incorporating prior knowledge in machine learning applications within astronomy and other scientific fields.

Acknowledgements

We thank Petr Baklanov for the discussion on multi-peaked SLSNe. T. Semenikhin acknowledges support from a Russian Science Foundation grant 24-22-00233, <https://rscf.ru/en/project/24-22-00233/>. Support was provided by Schmidt Sciences, LLC. for K. Malanchev.

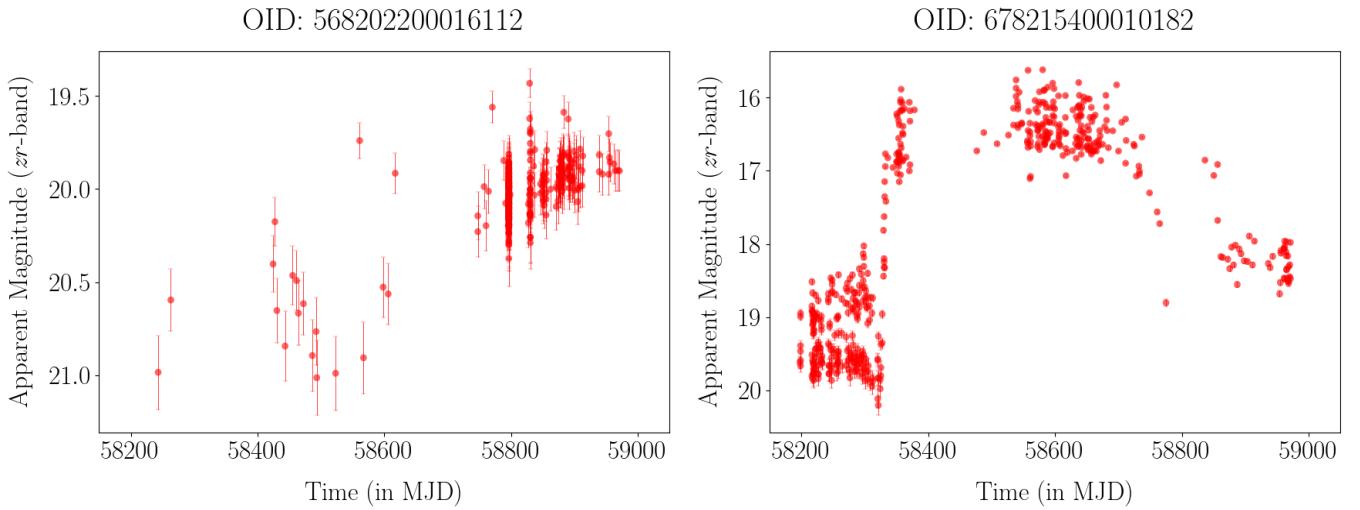


Figure 3: Outliers identified during the SLSN search using the `Pineforest` algorithm with priors. The left image shows a QSO (OID: 568202200016112) and the right image shows AM Herculis-type variable BM CrB (OID: 678215400010182). The photometry corresponds to MJD range of $58194.0 \leq \text{MJD} \leq 59524.0$, indicating the specific data used to extract features for the `Pineforest` algorithm.

Appendix A. Table of SLSN candidates

We present here a complete list of potential superluminous supernova candidates found with the PineForest active learning algorithm compiled with 8 SLSN light curves as priors present in the ZTF DR8.

TNS Name	Type ¹¹	RA (deg)	Dec (deg)	E(B-V)	z^{12}	$m_{r,\text{ref}}$	$M_{r,\text{peak}}$	$m_{r,\text{peak}}^{\text{GP}}$	$t_{0,\text{peak}}^{\text{GP}} (\text{MJD})$	Notes ¹³	
SN 2018dfa	SN IIP	230.21706	54.21550	0.01	0.125 (sp)	20.62 ± 0.02^{14}	-21.72 ± 0.11	18.84 ± 0.11	58 350.4	<i>zr</i> (794208200041246 , 794208200022136, 793205100013372), <i>zg</i> (793105100016413, 794108200005886) <i>zi</i> (793305100004986, 794308200006125, 793305100004986)	
SN 2018fcg	SLSN-I	317.40323	33.48323	0.17	0.101 (sp)	22.16 ± 0.08^{14}	-21.62 ± 0.01	18.44 ± 0.01	58 358.6	<i>zg</i> (689112300050742, 1729101400031561), <i>zr</i> (689212300032140 , 688209400039752, 1729201400023934)	
SN 2019bmj	SN II	220.29211	39.07256	0.01	0.054 (sp)	20.42 ± 0.05^{15}	-19.65 ± 0.03	18.81 ± 0.03	58 547.1	<i>zg</i> (719106400010004, 1718115300003331), <i>zr</i> (719206400011472 , 1718215300013528), <i>zi</i> (719306400018961)	
∞	AT 2019sez	–	134.15154	9.06560	0.04	0.114 ± 0.063 (ph)	20.75 ± 0.07^{15}	-19.48 ± 0.12	19.23±0.03	58 747.5	<i>zg</i> (518103200003350, 1512110400000162), <i>zr</i> (518203200005199 , 1512210400000179), <i>zi</i> (518303200012269)
AT 2019nkc	–	235.19183	38.84521	0.02	0.109 ± 0.064 (ph)	20.81 ± 0.05^{15}	-22.74 ± 0.17	17.50 ± 0.11	58 751.3	<i>zg</i> (721107400003558), <i>zr</i> (721207400007544), <i>zi</i> (721307400020258)	
AT 2019tjf	–	135.74812	15.48116	0.04	0.207 ± 0.092 (ph)	20.49 ± 0.06^{15}	-21.02 ± 0.19	19.11 ± 0.16	58 655.0	<i>zg</i> (518115100011724, 1564111400009400), <i>zr</i> (569204400026517 , 518215100006445, 1564211400013565), <i>zi</i> (518315100017723, 569304400003869)	

¹¹Classification is taken from the TNS based on its availability.

¹²All spectroscopic (sp) redshifts are obtained from the TNS, while photometric (ph) redshifts are sourced from <https://www.legacysurvey.org/viewer/>.

¹³The highlighted ZTF OIDs are obtained during the human-in-the-loop iterations.

¹⁴Pan-STARRS DR2 magnitude (Flewelling et al., 2020)

¹⁵ZTF reference magnitude

AT 2018moa	-	207.16852	63.57014	0.02	0.429 ± 0.381 (ph)	20.17 ± 0.02^{14}	-24.13 ± 0.24	19.46 ± 0.14	58 198.4	<i>zg</i> (821110200001558), <i>zr</i> (821210200003351 , 185220210000983), <i>zi</i> (821310200020112)
AT 2018mob	-	205.98618	64.60320	0.02	0.181 ± 0.040 (ph)	20.19 ± 0.02^{14}	-20.94 ± 0.07	20.50 ± 0.05	58 245.0	<i>zg</i> (821115400006169), <i>zr</i> (821215400003803 , 1852206300001446), <i>zi</i> (821315400015085)

Appendix B. Data Distribution of the Features Space and Priors

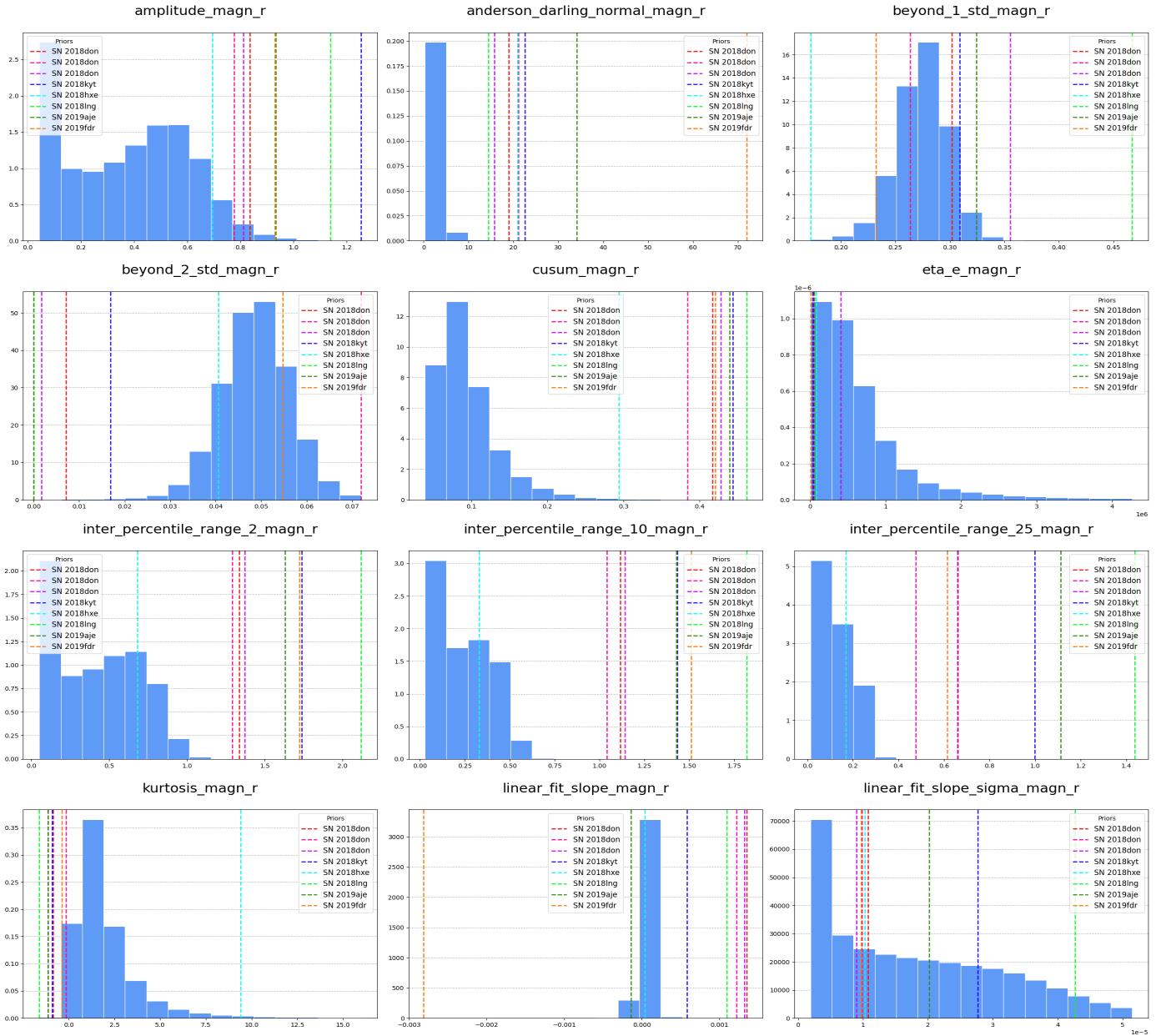


Figure B.4: The feature space distribution from the ZTF DR8 alongside the eight priors detailed in Table 1. The features are extracted using the light-curve package and focus on various magnitude properties, including Amplitude, Anderson-Darling Normal, Beyond N Std, Cusum, EtaE, Interpercentile Range, Kurtosis, and Linear Fit. The 8 horizontal dashed lines represent the feature values for each light curves as priors.

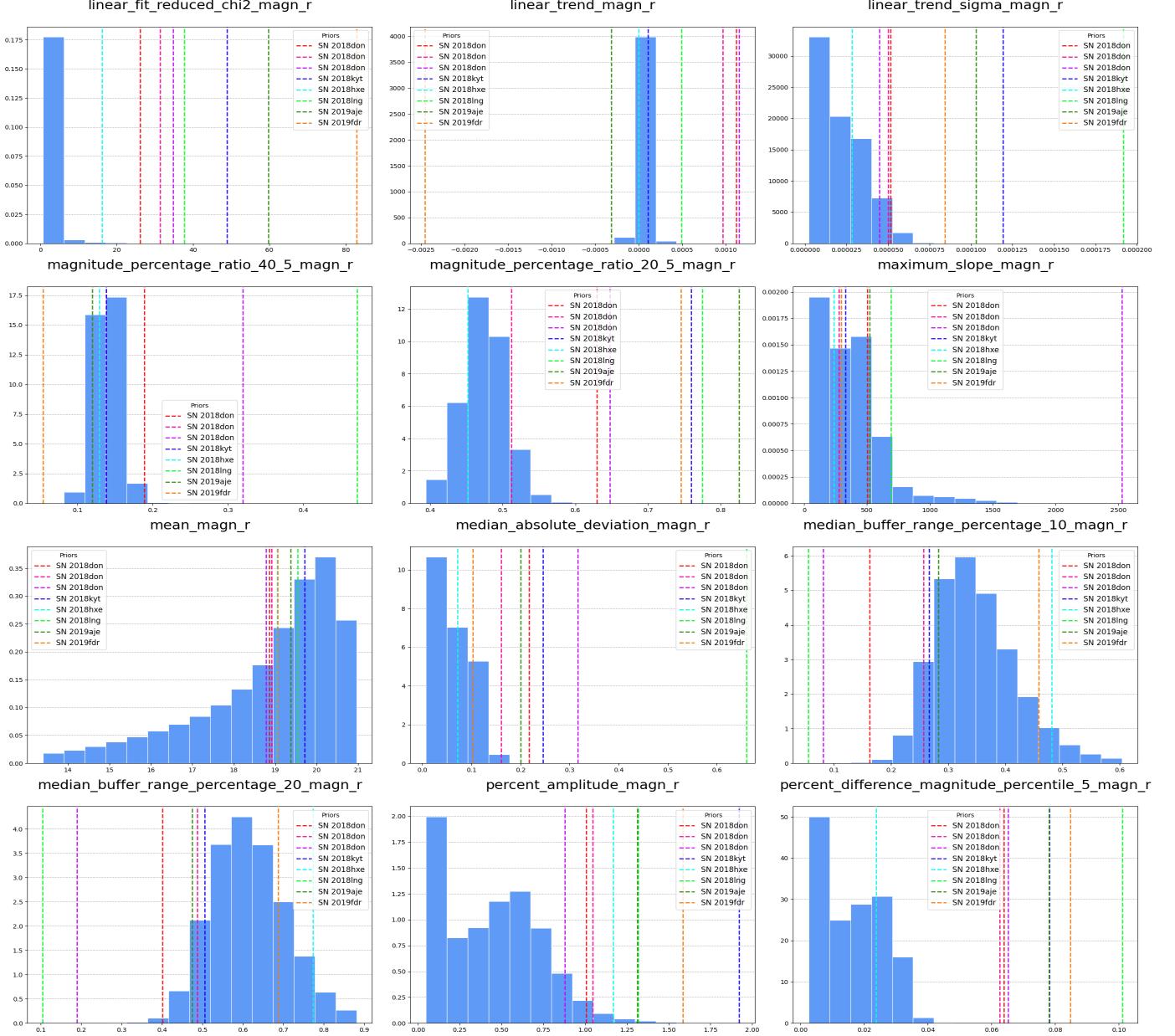


Figure B.5: The feature space distribution from the ZTF DR8 alongside the eight priors detailed in Table 1. The features are extracted using the light-curve package and focus on various magnitude properties, including Linear Fit, Linear Trend, MagnitudePercentageRatio, MaximumSlope, Mean, MedianAbsoluteDeviation, MedianBufferRangePercentage, PercentAmplitude, and PercentDifferenceMagnitudePercentile. The 8 horizontal dashed lines represent the feature values for each light curves as priors.

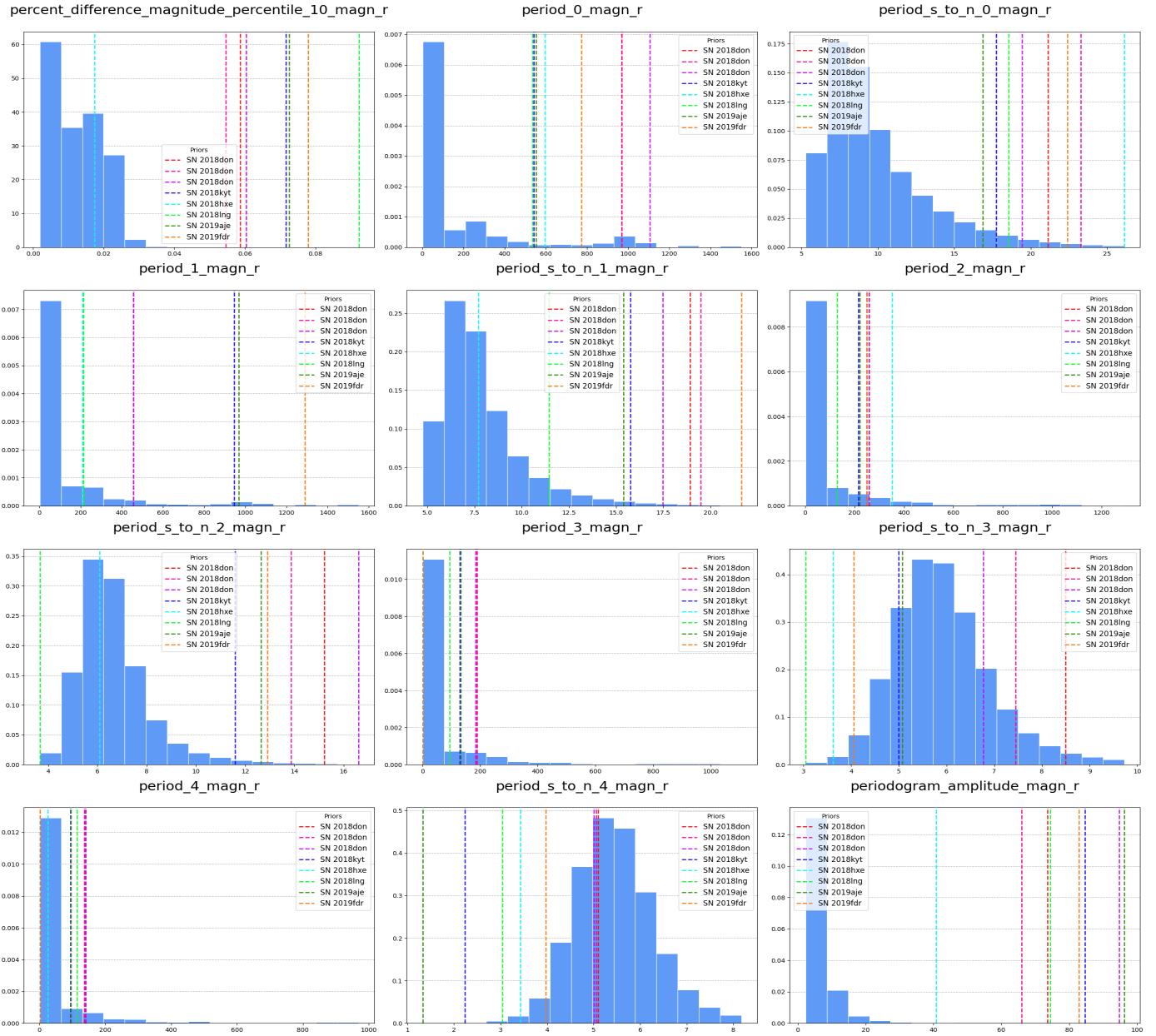


Figure B.6: The feature space distribution from the ZTF DR8 alongside the eight priors detailed in Table 1. The features are extracted using the `light-curve` package and focus on various magnitude properties, including `PercentDifferenceMagnitudePercentile` and `Periodogram`. The 8 horizontal dashed lines represent the feature values for each light curves as priors.

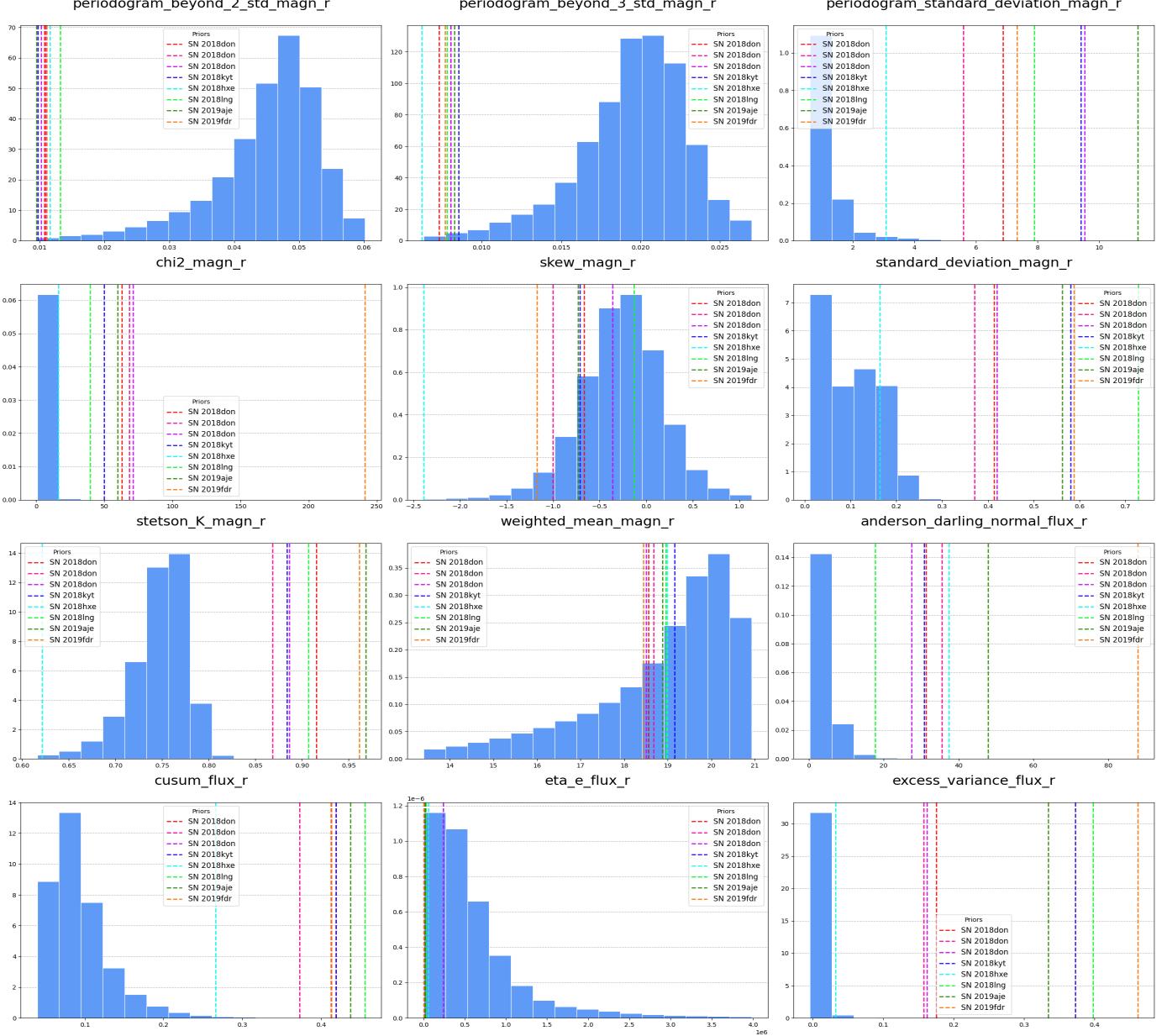


Figure B.7: The feature space distribution from the ZTF DR8 alongside the eight priors detailed in Table 1. The features are extracted using the `light-curve` package and focus on various magnitude properties, including Periodogram, ReducedChi2, Skew, StandardDeviation, StetsonK, and WeightedMean. Additionally, it includes flux properties like Anderson-Darling Normal, Cusum, EtaE, and ExcessVariance. The 8 horizontal dashed lines represent the feature values for each light curves as priors.

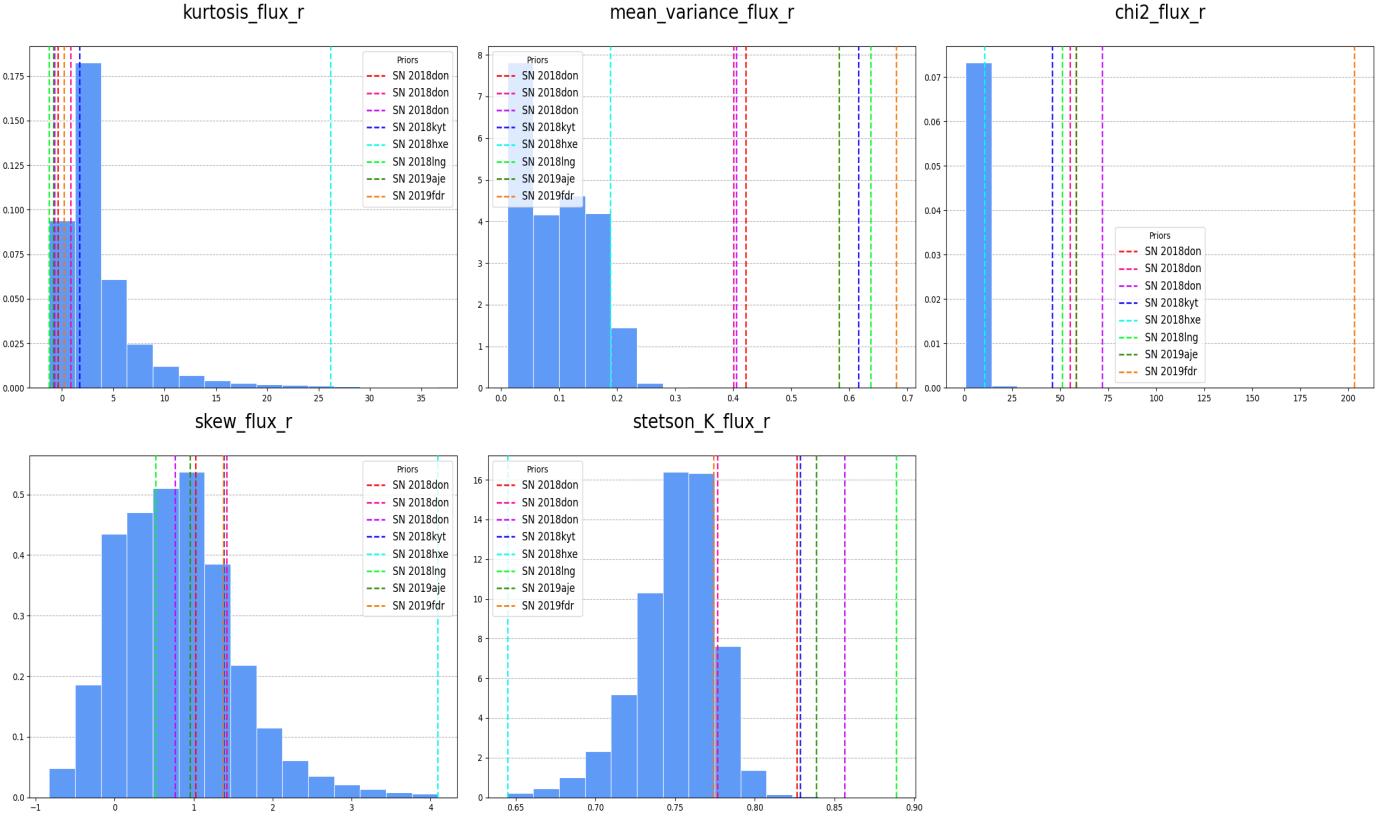


Figure B.8: The feature space distribution from the ZTF DR8 alongside the eight priors detailed in Table 1. The features are extracted using the `light-curve` package and focus on various flux properties, including Kurtosis, MeanVariance, ReducedChi2, Skew, and StetsonK. The 8 horizontal dashed lines represent the feature values for each light curves as priors.

References

- Aleo, P.D., Engel, A.W., Narayan, G., Angus, C.R., Malanchev, K., Auchettl, K., Baldassare, V.F., Berres, A., de Boer, T.J.L., Boyd, B.M., Chambers, K.C., Davis, K.W., Esquivel, N., Farias, D., Foley, R.J., Gagliano, A., Gall, C., Gao, H., Gomez, S., Grayling, M., Jones, D.O., Lin, C.C., Magnier, E.A., Mandel, K.S., Matheson, T., Raimundo, S.I., Shah, V.G., Soraisam, M.D., de Soto, K.M., Vicencio, S., Villar, V.A., Wainscoat, R.J., 2024. Anomaly Detection and Approximate Similarity Searches of Transients in Real-time Data Streams. *ApJ* 974, 172. doi:10.3847/1538-4357/ad6869, arXiv:2404.01235.
- Andersson, A., Lintott, C., Fender, R., Lochner, M., Woudt, P., van den Eijnden, J., van der Horst, A., Horesh, A., Saikia, P., Sivakoff, G.R., Tremou, L., Vaccari, M., 2024. Finding radio transients with anomaly detection and active learning based on volunteer classifications. arXiv e-prints , arXiv:2410.01034doi:10.48550/arXiv.2410.01034, arXiv:2410.01034.
- Baron, D., 2019. Machine Learning in Astronomy: a practical overview. arXiv e-prints , arXiv:1904.07248doi:10.48550/arXiv.1904.07248, arXiv:1904.07248.
- Bellm, E.C., Kulkarni, S.R., Graham, M.J., Dekany, R., Smith, R.M., Ridder, R., Masci, F.J., Helou, G., Prince, T.A., Adams, S.M., Barbarino, C., Barlow, T., Bauer, J., Beck, R., Belicki, J., Biswas, R., Blagorodnova, N., Bodewits, D., Bolin, B., Brinnel, V., Brooke, T., Bue, B., Bulla, M., Burruß, R., Cenko, S.B., Chang, C.K., Connolly, A., Coughlin, M., Cromer, J., Cunningham, V., De, K., Delacroix, A., Desai, V., Duev, D.A., Eadie, G., Farnham, T.L., Feeney, M., Feindt, U., Flynn, D., Franckowiak, A., Frederick, S., Fremling, C., Gal-Yam, A., Gezari, S., Giomi, M., Goldstein, D.A., Golkhou, V.Z., Goobar, A., Groom, S., Hacopians, E., Hale, D., Henning, J., Ho, A.Y.Q., Hover, D., Howell, J., Hung, T., Huppenkothen, D., Imel, D., Ip, W.H., Željko Ivezić, Jackson, E., Jones, L., Juric, M., Kasliwal, M.M., Kaspi, S., Kaye, S., Kelley, M.S.P., Kowalski, M., Kramer, E., Kupfer, T., Landry, W., Laher, R.R., Lee, C.D., Lin, H.W., Lin, Z.Y., Lunan, R., Giomi, M., Mahabal, A., Mao, P., Miller, A.A., Monkewitz, S., Murphy, P., Ngeow, C.C., Nordin, J., Nugent, P., Ofek, E., Patterson, M.T., Penprase, B., Porter, M., Rauch, L., Rebbapragada, U., Reiley, D., Rigault, M., Rodriguez, H., van Roestel, J., Rusholme, B., van Santen, J., Schulze, S., Shupe, D.L., Singer, L.P., Soumagnac, M.T., Stein, R., Surace, J., Sollerman, J., Szkody, P., Taddia, F., Terek, S., Sistine, A.V., van Velzen, S., Vestrand, W.T., Walters, R., Ward, C., Ye, Q.Z., Yu, P.C., Yan, L., Zolkower, J., 2018. The zwicky transient facility: System overview, performance, and first results. Publications of the Astronomical Society of the Pacific 131, 018002. URL: <https://dx.doi.org/10.1088/1538-3873/aaecbe>, doi:10.1088/1538-3873/aaecbe.
- Boch, T., Fernique, P., Manset, N., Forshay, P., 2014. Astronomical data analysis software and systems xxiii, in: in ASP Conf. ser., p. 277.
- Bonnarel, F., Fernique, P., Bienaymé, O., Egret, D., Genova, F., Louys, M., Ochsenbein, F., Wenger, M., Bartlett, J. G., 2000. The aladin interactive sky atlas - a reference tool for identification of astronomical sources. *Astron. Astrophys. Suppl. Ser.* 143, 33–40. URL: <https://doi.org/10.1051/aas:2000331>, doi:10.1051/aas:2000331.
- Das, S., Wong, W.K., Fern, A., Dietterich, T.G., Amran Siddiqui, M., 2017. Incorporating Feedback into Tree-based Anomaly Detection, in: Workshop on Interactive Data Exploration and Analytics (IDEA'17), p. arXiv:1708.09441. arXiv:1708.09441.
- Flewelling, H.A., Magnier, E.A., Chambers, K.C., Heasley, J.N., Holmberg, C., Huber, M.E., Sweeney, W., Waters, C.Z., Calamida, A., Casertano, S., Chen, X., Farrow, D., Hasinger, G., Henderson, R., Long, K.S., Metcalfe, N., Narayan, G., Nieto-Santisteban, M.A., Norberg, P., Rest, A., Saglia, R.P., Szalay, A., Thakar, A.R., Tonry, J.L., Valenti, J., Werner, S., White, R., Denneau, L., Draper, P.W., Hodapp, K.W., Jedicke, R., Kaiser, N., Kudritzki, R.P., Price, P.A., Wainscoat, R.J., Chastel, S., McLean, B., Postman, M., Shiao, B., 2020. The pan-starrs1 database and data products. *The Astrophysical Journal Supplement Series* 251, 7. URL: <https://dx.doi.org/10.3847/1538-4365/abb82d>, doi:10.3847/1538-4365/abb82d.
- Forestano, R.T., Matchev, K.T., Matcheva, K., Unlu, E.B., 2023. Searching for Novel Chemistry in Exoplanetary Atmospheres Using Machine Learning for Anomaly Detection. *ApJ* 958, 106. doi:10.3847/1538-4357/ad0047, arXiv:2308.07604.
- Fremling, C., Sharma, Y., Dugas, A., 2018. ZTF Transient Classification Report for 2018-08-04. Transient Name Server Classification Report 2018-1100, 1.
- Gaia Collaboration, Vallenari, A., Brown, A. G. A., Prusti, T., de Bruijne, J. H. J., Arenou, F., Babusiaux, C., Biermann, M., Creevey, O. L., Ducourant, C., Evans, D. W., Eyer, L., Guerra, R., Hutton, A., Jordi, C., Klioner, S. A., Lammers, U. L., Lindegren, L., Luri, X., Mignard, F., Panem, C., Pourbaix, D., Randich, S., Sartoretti, P., Soubiran, C., Tanga, P., Walton, N. A., Bailer-Jones, C. A. L., Bastian, U., Drimmel, R., Jansen, F., Katz, D., Lattanzi, M. G., van Leeuwen, F., Bakker, J., Cacciari, C., Castañeda, J., De Angeli, F., Fabricius, C., Fouesneau, M., Frémat, Y., Galluccio, L., Guerrier, A., Heiter, U., Masana, E., Messineo, R., Mowlavi, N., Nicolas, C., Nienartowicz, K., Pailler, F., Panuzzo, P., Riclet, F., Roux, W., Seabroke, G. M., Sordo, R., Thévenin, F., Gracia-Abril, G., Portell, J., Teyssier, D., Altmann, M., Andrae, R., Audard, M., Bellas-Velidis, I., Benson, K., Berthier, J., Blomme, R., Burgess, P. W., Busonero, D., Busso, G., Cánovas, H., Carry, B., Cellino, A., Cheek, N., Clementini, G., Damerdji, Y., Davidson, M., de Teodoro, P., Nuñez Campos, M., Delchambre, L., Dell’Oro, A., Esquej, P., Fernández-Hernández, J., Fraile, E., Garabato, D., García-Lario, P., Gosset, E., Haigron, R., Halbwachs, J.-L., Hamby, N. C., Harrison, D. L., Hernández, J., Hestroffer, D., Hodgkin, S. T., Holl, B., Janßen, K., Jevardat de Fombelle, G., Jordan, S., Krone-Martins, A., Lanzafame, A. C., Löffler, W., Marchal, O., Marrese, P. M., Moitinho, A., Muinonen, K., Osborne, P., Pancino, E., Pauwels, T., Recio-Blanco, A., Reyillé, C., Riello, M., Rimoldini, L., Roegiers, T., Rybizki, J., Sarro, L. M., Siopis, C., Smith, M., Sozzetti, A., Utrilla, E., van Leeuwen, M., Abbas, U., Ábrahám, P., Abreu Aramburu, A., Aerts, C., Aguado, J. J., Ajaj, M., Aldea-Montero, F., Al tavilla, G., Álvarez, M. A., Alves, J., Anders, F., Anderson, R. I., Anglada Varela, E., Antoja, T., Baines, D., Baker, S. G., Balaguer-Núñez, L., Balbinot, E., Balog, Z., Barache, C., Barbato, D., Barros, M., Barstow, M. A., Bartolomé, S., Bassilana, J.-L., Bauchet, N., Becciani, U., Bellazzini, M., Berihuete, A., Bernet, M., Bertone, S., Bianchi, L., Binnenfeld, A., Blanco-Cuaresma, S., Blazere, A., Boch, T., Bombrun, A., Bossini, D., Bouquillon, S., Bragaglia, A., Bramante, L., Breedt, E., Bressan, A., Brouillet, N., Brugaletta, E., Bucciarelli, B., Burlacu, A., Butkevich, A. G., Buzzi, R., Caffau, E., Cancilliere, R., Cantat-Gaudin, T., Carballo, R., Carlucci, T., Carnerero, M. I., Carrasco, J. M., Casamiquela, L., Castellani, M., Castro-Ginard, A., Chaoul, L., Charlot, P., Chemin, L., Chiaramida, V., Chiavassa, A., Chornay, N., Comoretto, G., Contursi, G., Cooper, W. J., Cornez, T., Cowell, S., Crifo, F., Cropper, M., Crosta, M., Crowley, C., Dafonte, C., Dapergolas, A., David, M., David, P., de Laverny, P., De Luise, F., De March, R., De Ridder, J., de Souza, R., de Torres, A., del Peloso, E. F., del Pozo, E., Delbo, M., Delgado, A., Delisle, J.-B., Demouchy, C., Dharmawardena, T. E., Di Matteo, P., Diakite, S., Diener, C., Distefano, E., Dolding, C., Edvardsson, B., Enke, H., Fabre, C., Fabrizio, M., Faigler, S., Fedorets, G., Fernique, P., Fienga, A., Figueras, F., Fournier, Y., Fouron, C., Frakoudi, F., Gai, M., Garcia-Gutierrez, A., Garcia-Reinaldos, M., García-Torres, M., Garofalo, A., Gavel, A., Gavras, P., Gerlach, E., Geyer, R., Giacobbe, P., Gilmore, G., Girona, S., Giuffrida, G., Golmel, R., Gomez, A., González-Núñez, J., González-Santamaría, I., González-Vidal, J. J., Granvik, M., Guillout, P., Guiraud, J., Gutiérrez-Sánchez, R., Guy, L. P., Hatzidimitriou, D., Hauser, M., Haywood, M., Helmer, A., Helmi, A., Sarmiento, M. H., Hidalgo, S. L., Hilger, T., Hładcuk, N., Hobbs, D., Holland, G., Huckle, H. E., Jardine, K., Jasniewicz, G., Jean-Antoine Piccolo, A., Jiménez-Arranz, Ó., Jorissen, A., Juaristi Campillo, J., Julbe, F., Karbevska, L., Kervella, P., Khanna, S., Kontizas, M., Kordopatis, G., Korn, A. J., Kóspál, Á., Kostrzewa-Rutkowska, Z., Kruszyńska, K., Kun, M., Laizeau, P., Lambert, S., Lanza, A. F., Lasne, Y., Le Campion, J.-F., Lebreton, Y., Lebzelter, T., Leccia, S., Leclerc, N., Lecoeur-Taibi, I., Liao, S., Licata, E. L., Lindström, H. E. P., Lister, T. A., Livanou, E., Lobel, A., Lorca, A., Loup, C., Madrero Pardo, P., Magdaleno Romeo, A., Managau, S., Mann, R. G., Manteiga, M., Marchant, J. M., Marconi, M., Marcos, J., Marcos Santos, M. M. S., Marín Pina, D., Marinoni, S., Marocco, F., Marshall, D. J., Martin Polo, L., Martín-Fleitas, J. M., Marton, G., Mary, N., Masip, A., Massari, D., Mastrobuono-Battisti, A., Mazeh, T., McMillan, P. J., Messina, S., Michalik, D., Millar, N. R., Mints, A., Molina, D., Molinaro, R., Molnár, L., Monari, G., Monguió, M., Montegriffo, P., Montero, A., Mor, R., Mora, A., Morbidelli, R., Morel, T., Morris, D., Mureaveva, T., Murphy, C. P., Musella, I., Nagy, Z., Noval, L., Ocaña, F., Ogden, A., Ordenovic, C., Osinde, J. O., Pagani, C., Pagano, I., Palaversa, L., Palacio, P. A., Pallas-Quintela, L., Panahi, A., Payne-Wardenaar, S., Peñalosa Esteller, X., Penttilä, A., Pichon, B., Piersimoni, A. M., Pineau, F.-X., Plachy, E., Plum, G., Poggio, E., Prša, A., Pulone, L., Racero, E., Ragaini, S., Rainer, M., Raiteri, C. M., Rambaux, N., Ramos, P., Ramos-Lerate, M., Re Fiorentin, P., Regibo, S., Richards, P. J., Rios Diaz, C., Ripepi, V., Riva,

- A., Rix, H.-W., Rixon, G., Robichon, N., Robin, A. C., Robin, C., Roelens, M., Rogues, H. R. O., Rohrbasser, L., Romero-Gómez, M., Rowell, N., Royer, F., Ruiz-Mieres, D., Rybicki, K. A., Sadowski, G., Sáez Núñez, A., Sagristà Sellés, A., Sahlmann, J., Salguero, E., Samaras, N., Sanchez Giménez, V., Sanna, N., Santovenia, R., Sarasso, M., Schultheis, M., Sciaccà, E., Segol, M., Segovia, J. C., Ségransan, D., Semeux, D., Shahaf, S., Siddiqui, H. I., Siebert, A., Siltala, L., Silvelo, A., Slezak, E., Slezak, I., Smart, R. L., Snaith, O. N., Solano, E., Solitro, F., Souami, D., Souchay, J., Spagna, A., Spina, L., Spoto, F., Steele, I. A., Steidelmüller, H., Stephenson, C. A., Süveges, M., Surdej, J., Szabados, L., Szegedi-Elek, E., Taris, F., Taylor, M. B., Teixeira, R., Tolomei, L., Tonello, N., Torra, F., Torra, J., Torralba Elipe, G., Trabucchi, M., Tsounis, A. T., Turon, C., Ulla, A., Unger, N., Vaillant, M. V., van Dillen, E., van Reeven, W., Vanel, O., Vecchiato, A., Viala, Y., Vicente, D., Voutsinas, S., Weiler, M., Wevers, T., Wyrzykowski, Ł., Yoldas, A., Yvard, P., Zhao, H., Zorec, J., Zucker, S., Zwitter, T., 2023. Gaia data release 3 - summary of the content and survey properties. *A&A* 674, A1. URL: <https://doi.org/10.1051/0004-6361/202243940>, doi:10.1051/0004-6361/202243940.
- Gal-Yam, A., 2012. Luminous Supernovae. *Science* 337, 927. doi:10.1126/science.1203601, arXiv:1208.3217.
- Gal-Yam, A., 2019. The most luminous supernovae. *Annual Review of Astronomy and Astrophysics* 57, 305–333. URL: <https://doi.org/10.1146/annurev-astro-081817-051819>, doi:10.1146/annurev-astro-081817-051819.
- Horton, P., Thompson, C., Groppi, C., Seo, Y., Siles, J.V., 2024. On-board science data quality analysis using anomaly detection for ASTHROS, in: Zmuidzinas, J., Gao, J.R. (Eds.), Society of Photo-Optical Instrumentation Engineers (SPIE) Conference Series, p. 1310212. doi:10.1117/12.3017661.
- Ishida, E.E.O., Kornilov, M.V., Malanchev, K.L., Pruzhinskaya, M.V., Volnova, A.A., Korolev, V.S., Mondon, F., Sreejith, S., Malancheva, A.A., Das, S., 2021. Active anomaly detection for time-domain discoveries. *A&A* 650, A195. doi:10.1051/0004-6361/202037709, arXiv:1909.13260.
- Kornilov, M.V., Korolev, V.S., Malanchev, K.L., Lavrukhina, A.D., Russeil, E., Semenikhin, T.A., Gangler, E., Ishida, E.E.O., Pruzhinskaya, M.V., Volnova, A.A., Sreejith, S., 2024. Coniferest: a complete active anomaly detection framework. arXiv e-prints , arXiv:2410.17142doi:10.48550/arXiv.2410.17142, arXiv:2410.17142.
- Liu, F.T., Ting, K.M., Zhou, Z.H., 2008. Isolation forest, in: 2008 Eighth IEEE International Conference on Data Mining, pp. 413–422. doi:10.1109/ICDM.2008.17.
- Lochner, M., Bassett, B.A., 2021. ASTRONOMALY: Personalised active anomaly detection in astronomical data. *Astronomy and Computing* 36, 100481. doi:10.1016/j.ascom.2021.100481, arXiv:2010.11202.
- Malanchev, K., Kornilov, M.V., Pruzhinskaya, M.V., Ishida, E.E.O., Aleo, P.D., Korolev, V.S., Lavrukhina, A., Russeil, E., Sreejith, S., Volnova, A.A., Voloshina, A., Krone-Martins, A., 2023. The snad viewer: Everything you want to know about your favorite ztf object. *Publications of the Astronomical Society of the Pacific* 135, 024503. URL: <https://dx.doi.org/10.1088/1538-3873/acb292>, doi:10.1088/1538-3873/acb292.
- Malanchev, K.L., Pruzhinskaya, M.V., Korolev, V.S., Aleo, P.D., Kornilov, M.V., Ishida, E.E.O., Krushinsky, V.V., Mondon, F., Sreejith, S., Volnova, A.A., Belinski, A.A., Dodin, A.V., Tatarnikov, A.M., Zheltoukhov, S.G., (The SNAD Team), 2021. Anomaly detection in the Zwicky Transient Facility DR3. *MNRAS* 502, 5147–5175. doi:10.1093/mnras/stab316, arXiv:2012.01419.
- Mesarcik, M., Boonstra, A.J., Iacobelli, M., Rangelova, E., de Laat, C.T.A.M., van Nieupoort, R.V., 2023. The ROAD to discovery: Machine-learning-driven anomaly detection in radio astronomy spectrograms. *A&A* 680, A74. doi:10.1051/0004-6361/202347182, arXiv:2307.01054.
- Moriya, T.J., Sorokina, E.I., Chevalier, R.A., 2018. Superluminous Supernovae. *Space Sci. Rev.* 214, 59. doi:10.1007/s11214-018-0493-6, arXiv:1803.01875.
- Parmiggiani, N., Bulgarelli, A., Ursi, A., Macaluso, A., Di Piano, A., Fioretti, V., Aboudan, A., Baroncelli, L., Addis, A., Tavani, M., Pittori, C., 2023. A Deep-learning Anomaly-detection Method to Identify Gamma-Ray Bursts in the Ratemeters of the AGILE Anticoincidence System. *ApJ* 945, 106. doi:10.3847/1538-4357/acba0a.
- Perez-Carrasco, M., Cabrera-Vives, G., Hernandez-García, L., Förster, F., Sanchez-Saez, P., Muñoz Arancibia, A.M., Arredondo, J., Astorga, N., Bauer, F.E., Bayo, A., Catelan, M., Dastidar, R., Estévez, P.A., Lira, P., Pignata, G., 2023. Alert Classification for the ALeRCE Broker System: The Anomaly Detector. *AJ* 166, 151. doi:10.3847/1538-3881/ace0c1.
- Pessi, P.J., Lunnan, R., Sollerman, J., Schulze, S., Gkini, A., Gangopadhyay, A., Yan, L., Gal-Yam, A., Perley, D.A., Chen, T.W., Hinds, K.R., Brennan, S.J., Hu, Y., Singh, A., Andreoni, I., Cook, D.O., Fremling, C., Ho, A.Y.Q., Sharma, Y., van Velzen, S., Wold, A., Bellm, E.C., Bloom, J.S., Graham, M.J., Kasliwal, M.M., Kulkarni, S.R., Riddle, R., Rusholme, B., 2024. Sample of hydrogen-rich superluminous supernovae from the Zwicky Transient Facility. arXiv e-prints , arXiv:2408.15086doi:10.48550/arXiv.2408.15086, arXiv:2408.15086.
- Pruzhinskaya, M.V., Ishida, E.E.O., Novinskaya, A.K., Russeil, E., Volnova, A.A., Malanchev, K.L., Kornilov, M.V., Aleo, P.D., Korolev, V.S., Krushinsky, V.V., Sreejith, S., Gangler, E., 2023. Supernova search with active learning in ZTF DR3. *A&A* 672, A111. doi:10.1051/0004-6361/202245172, arXiv:2208.09053.
- Sánchez-Sáez, P., Lira, H., Martí, L., Sánchez-Pi, N., Arredondo, J., Bauer, F.E., Bayo, A., Cabrera-Vives, G., Donoso-Oliva, C., Estévez, P.A., Eyheramendy, S., Förster, F., Hernández-García, L., Arancibia, A.M.M., Pérez-Carrasco, M., Sepúlveda, M., Vergara, J.R., 2021. Searching for Changing-state AGNs in Massive Data Sets. I. Applying Deep Learning and Anomaly-detection Techniques to Find AGNs with Anomalous Variability Behaviors. *AJ* 162, 206. doi:10.3847/1538-3881/ac1426, arXiv:2106.07660.
- Schlafly, E.F., Finkbeiner, D.P., 2011. Measuring reddening with Sloan Digital Sky Survey stellar spectra and recalibrating sfd. *The Astrophysical Journal* 737, 103. URL: <http://dx.doi.org/10.1088/0004-637X/737/2/103>, doi:10.1088/0004-637X/737/2/103.
- Semenikhin, T.A., Kornilov, M.V., Pruzhinskaya, M.V., Lavrukhina, A.D., Russeil, E., Gangler, E., Ishida, E.E.O., Korolev, V.S., Malanchev, K.L., Volnova, A.A., Sreejith, S., 2024. Real-bogus scores for active anomaly detection. arXiv e-prints , arXiv:2409.10256doi:10.48550/arXiv.2409.10256, arXiv:2409.10256.
- Settles, B., 2012. Active Learning. Synthesis lectures on artificial intelligence and machine learning, Morgan & Claypool. URL: https://books.google.fr/books?id=z7toC3z_QjQC.
- Smith, N., Miller, A., Li, W., Filippenko, A.V., Silverman, J.M., Howard, A.W., Nugent, P., Marcy, G.W., Bloom, J.S., Ghez, A.M., Lu, J., Yelda, S., Bernstein, R.A., Colucci, J.E., 2010. Discovery of precursor luminous blue variable outbursts in two recent optical transients: The fitfully variable missing links ugc 2773-ot and sn 2009ip. *The Astronomical Journal* 139, 1451. URL: <https://dx.doi.org/10.1088/0004-6256/139/4/1451>, doi:10.1088/0004-6256/139/4/1451.
- Voloshina, A.S., Lavrukhina, A.D., Pruzhinskaya, M.V., Malanchev, K.L., Ishida, E.E.O., Krushinsky, V.V., Aleo, P.D., Gangler, E., Kornilov, M.V., Korolev, V.S., Russeil, E., Semenikhin, T.A., Sreejith, S., Volnova, A.A., team, T.S., 2024. SNAD catalogue of M-dwarf flares from the Zwicky Transient Facility. *Monthly Notices of the Royal Astronomical Society* 533, 4309–4323. URL: <https://doi.org/10.1093/mnras/stae2031>, doi:10.1093/mnras/stae2031, arXiv:<https://academic.oup.com/mnras/article-pdf/533/4/4309/5908733.pdf>
- Watson, C., Henden, A.A., Price, A., 2022. VizieR Online Data Catalog: AAVSO International Variable Star Index VSX (Watson+, 2006-). VizieR On-line Data Catalog: B/vsx. Originally published in: 2006SASS...25...47W.
- Wenger, M., Ochsenbein, F., Egret, D., Dubois, P., Bonnarel, F., Borde, S., Genova, F., Jasnewicz, G., Laloë, S., Lesteven, S., Monier, R., 2000. The SIMBAD astronomical database. The CDS reference database for astronomical objects. *A&AS* 143, 9–22. doi:10.1051/aas:2000332, arXiv:astro-ph/0002110.
- Xiong, L., Poczos, B., Connolly, A., Schneider, J., 2010. Anomaly detection for astronomical data .